Electronic Supplementary Material (ESI) for Organic & Biomolecular Chemistry.

SUPPORTING INFORMATION

Selective Sensing of Al^{3+} Ion by nitrophenyl induced coordination: Imaging in Zebrafish Brain Tissue

Sujoy Das[†], Urmi Mukherjee[‡], Soumojit Pal[‡], Sudipta Maitra[‡] and Prithidipa Sahoo[*†]

[†]Department of Chemistry, Visva-Bharati University, Santiniketan, 731235, W.B., India.
[‡]Department of Zoology, Visva-Bharati University, Santiniketan, 731235, India.
*Corresponding author. E-mail: prithidipa@hotmail.com

Content

1. Table S1. Performance Comparison of Existing Methods And Present Method for fluorescence imaging of Aluminium (III) over the last decade using rhodamine based fluorescent chemosensors:

Analytes	Sensor type	Detection limit (μM)	Medium	Sensitvity & selectivity	Response Time	Estimation	Reference
Al^{3+}	**4-nitro aniline**	**0.3 μM (1:1)**	**CH_3CN/ H_2O (1:8)**	**high**	**2 min**	**Zebrafish brain tissue**	**This manuscript**
Al^{3+}	1,8-naphthalimide	0.1 μM (1:1)	H_2O - EtOH (99:1)	high	> 2 min	Hela cell	Sensors and Actuators B 186 (2013) 360–366.
Al^{3+}	Mesitylene-triazole	(1:1)	MeOH-H_2O (9:1)	moderate	30 min	No	Inorg. Chem. 2013, 52, 1161−1163.
Al^{3+}	diformyl p-cresol conjugate	5 nM (2:1)	H_2O - EtOH (1:4)	moderate	30 min	Pollen cells	Inorg. Chem. 2013, 52, 3627−3633
Al^{3+}	2,7-dimethoxy-9H-fluoren-9-one	2.4 μM (1:1)	MeOH-H_2O (3:7)	low	n.d.	No	Tetrahedron Letters 54 (2013) 3630–3634.
Al^{3+}	Rhodamine-azacrown derivative	12 nM/ 86 nM (1:1)/ (2:1)	H_2O - EtOH (4:1) and MeCN	Moderate	60 min	No	Dyes and Pigments 101 (2014) 58-66
Al^{3+}/ Cu^{2+}	2-methoxy cimnamaldehyde	8.3 nM (1:1)	Acetonitrile	Low	n.d.	No	Tetrahedron Letters 55 (2014) 4912–4916.
Al^{3+}	3-hydroxyl flavone	3.98 μM	CH_3CN/ H_2O (95:5)	Moderate-low	>2 h	yes	New J. Chem., 2015, 39, 342
Al^{3+}	sodium benzoate-rhodamine 6G	3.26 μM (2:1)	H_2O-EtOH (4 : 1)	high	n.d.	Hela cells	Dalton Trans., 2014, 43, 12624–12632.
Al^{3+}	2,3-dihydroxy benzaldehyde	20 nM (1:1)	CH_3CN/ H_2O (4:1)	high	Immediate	No	New J. Chem., 2014, 38, 1627-1634.
Al^{3+}	o-nitro benzaldehyde	60 nM (1:1)	EtOH-H_2O (1:3)	High	30 min	Hela cells, MCF-7	Dalton Trans., 2015, 44, 8708–8717.
Al^{3+}	Thiophosgene, piperazine	11 nM (1:1)	MeCN/ H_2O (1:1)	High	n.d.	No	Sensors and Actuators B Chemical, 220

							(2015) 1196-1204.
Al^{3+}	2-chloro nicotinaldehyde	28.6 nM (1:1)	MeCN/ H_2O	High	n.d.	No	Sensors and Actuators B: Chemical 208 (2015) 75-84.
Al^{3+}/ Ag^{+}	1-naphthalene isothiocyanate	1.27 μM (1:1)	MeCN/ H_2O (4:1)	Moderate	n.d.	Hela cells	Supramolecular Chemistry, 2015, 27, 490–500.
Al^{3+}	4-nitro salicylaldimine	0.44 μM (1:1)	DMSO/ H_2O (9:1)	Moderate	5 min	No	Sensors and Actuators B 222 (2016) 447–458.
Al^{3+}	Adenine	0.19 μM (1:1)	DMSO/ H_2O (1:4)	High	30 sec	Pollen and candida cells	Journal of Luminescence 169 (2016) 334–341.
Al^{3+}	5-methyl salicaldehyde	2.8 nM (1:1)	MeOH-H_2O (9:1)	high	Few seconds	prokaryotic and eukaryotic cells	New J. Chem., 2018, 42, 8415-8425.

2. Materials and Methods

Rhodamine B, *p*-nitro aniline, phosphoryl chloride, Aluminum nitrate and all other metal salts were purchased from Sigma-Aldrich Pvt. Ltd. (India). Unless otherwise mentioned, materials were obtained from commercial suppliers and were used without further purification. All the solvents were dried following the standard procedures. Elix Millipore water was used in all respective experiments. ^1H and ^{13}C NMR spectra were recorded on a Bruker 400 MHz instrument. For NMR spectra and for NMR titration DMSO-d_6 and D_2O were used as solvent using TMS as an internal standard. Chemical shifts are expressed in δ ppm units and ^1H–^1H and ^1H–C coupling constants in Hz. The mass spectrum (HRMS) was carried out using a micromass Q-TOF Micro™ instrument by using methanol as a solvent. Fluorescence spectra were recorded on a PerkinElmer Model LS55 spectrophotometer. UV spectra were recorded on a SHIMADZU UV-3101PC spectrophotometer. Elemental analysis of the compounds was carried out on Perkin-Elmer 2400 series CHNS/O Analyzer. The following abbreviations are used to describe spin multiplicities in ^1H NMR spectra: s = singlet; d = doublet; t = triplet; m = multiplet.

Preparation of NPRB: 0.25g (1.8 mmol) of *p*-nitroaniline was dissolved in a mixture of Rhodamine B (0.86 g, 1.8 mmol) and $POCl_3$ (0.5 mL) taken under nitrogen atmosphere. The reaction mixture was refluxed for 12 hours and poured into 25 ml of 5% aqueous $NaHCO_3$ Solution, extracted with $CHCl_3$. Organic layer was separated and dried over anhydrous Na_2SO_4. Crude product was further purified by column chromatography ($CHCl_3$:EtOAc = 7:1) to obtain the probe **NPRB** (0.79 g) with 79% yield (Figure S1). Melting point:-180ºC, Yield:-75%. ^1H NMR (DMSO-d_6, 400 MHz): d (ppm): 8.03-8.05 (d, 2H, J= 8 Hz), 7.92-7.95 (m, 1H, J = 12 Hz), 7.52-7.60 (m, 2H, J = 32 Hz), 7.44-7.46 (d, 2H, J= 8 Hz), 7.01-7.03 (d, 1H, J = 8 Hz), 6.53-6.55 (d, 2H, J = 8 Hz), 6.37 (s, 2H), 6.31-6.33 (d, 2H, J = 8 Hz), 3.25-

3.30 (m, 8H, J= 20 Hz), 1.03-1.06 (t, 12H, J = 12 Hz). ^{13}C NMR (DMSO-d_6, 400 MHz): δ (ppm)= 167.62, 153.84, 151.86, 148.51, 143.69, 143.44, 134.24, 128.63, 127.75, 124.02, 123.56, 123.26, 112.34, 108.36, 105.20, 97.37, 66.61, 43.59, 12.34. Anal.Calcd. For $C_{34}H_{34}N_4O_4$: C, 72.58; H, 6.09; N, 9.96; O, 11.37. Found: C, 72.45; H, 6.15; N, 9.5; O, 11.59. MALDI (TOF MS): Anal. calcd for $C_{34}H_{34}N_4O_4$: 562.26; found: 563.27 [M+H$^+$, 100%].

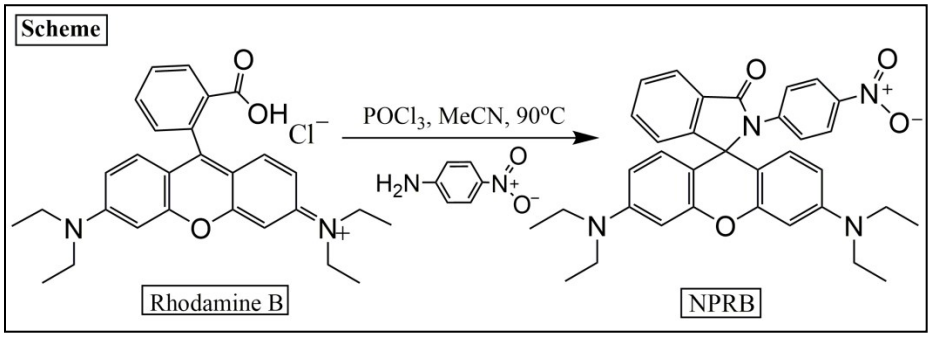

Figure S1. Synthesis of probe **NPRB**.

3. NMR Studies:

^{1}H NMR of NPRB in DMSO-d_6:

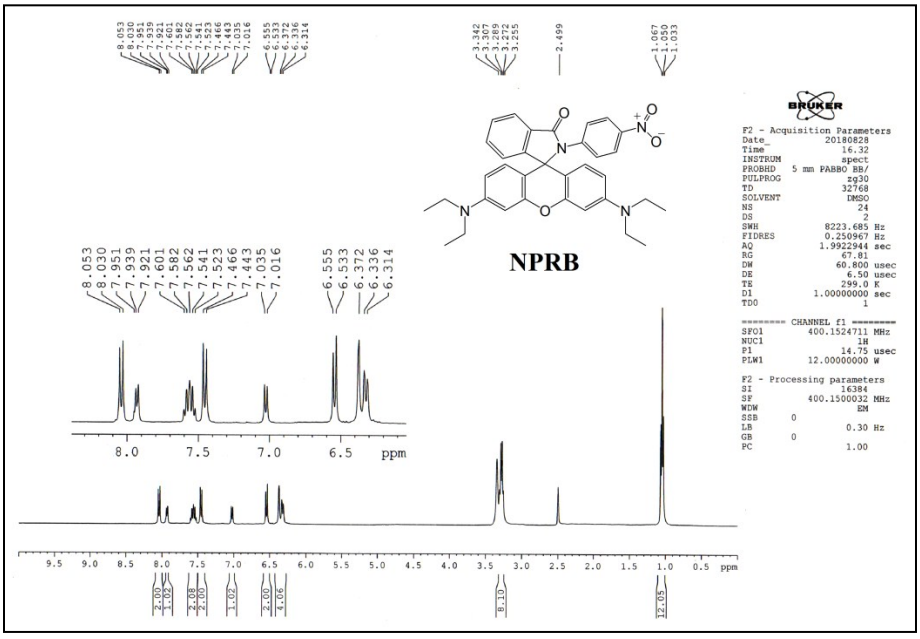

Figure S2. ^{1}H NMR of **NPRB** in DMSO-d_6 (400 MHz).

^{13}C NMR of NPRB in DMSO-d_6:

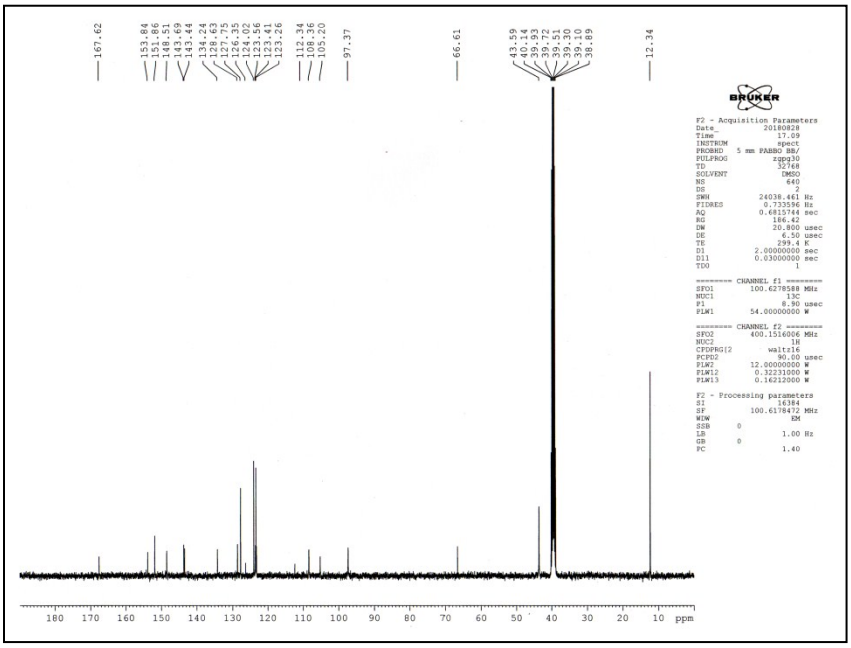

Figure S3. ^{13}C NMR of **NPRB** in DMSO-d_6 (400 MHz)

4. Mass spectrum of NPRB:

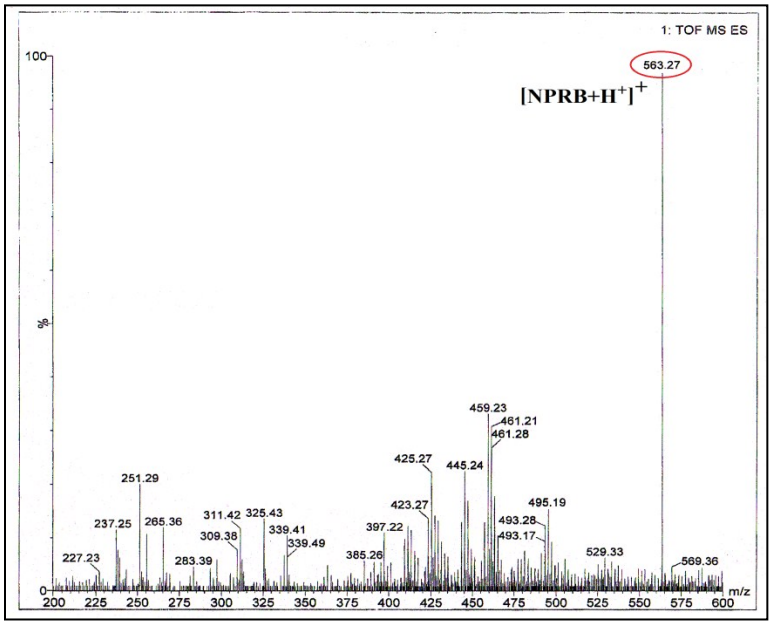

Figure S4. MALDI-TOF MS of **NPRB**.

5. Time dependent fluorescence changes of NPRB upon gradual addition of Al^{3+}:

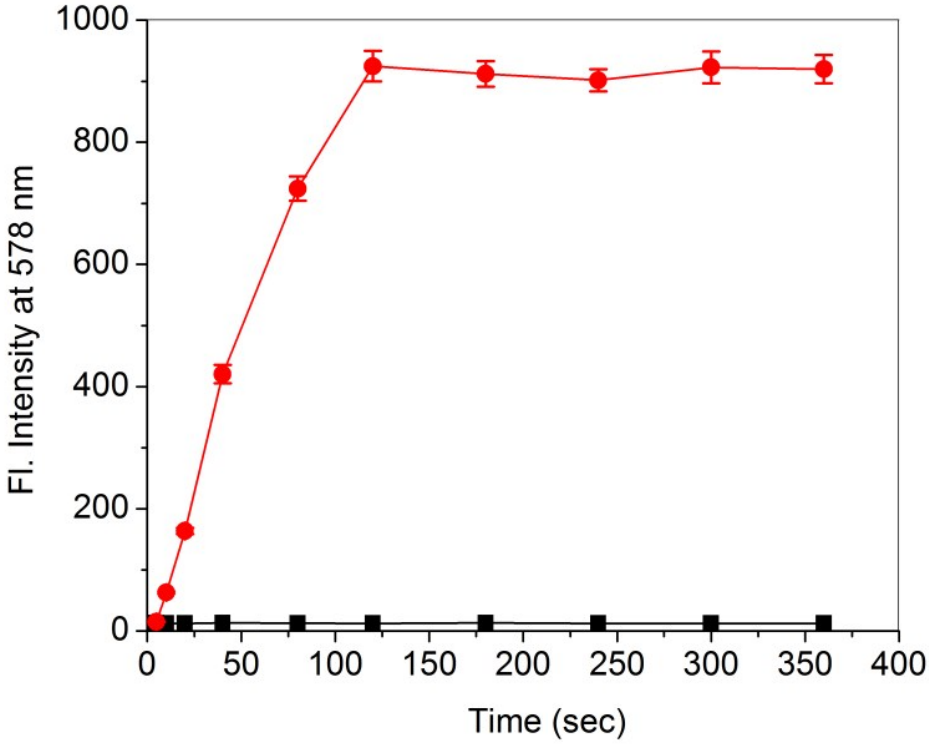

Figure S5. Fluorescence intensity plot of probe **NPRB** before (black) and after (red) addition of Al^{3+} upto 4 equiv. as a function of time in CH_3CN/H_2O (1:8, v/v) (λ_{ex}= 490 nm). Standard deviation are represented by error bars (n=3).

6. Evaluation of the Association constant and Limit of Detection (LOD) for the formation of NPRB-Al^{3+} complex:

Binding constant calculation graph:

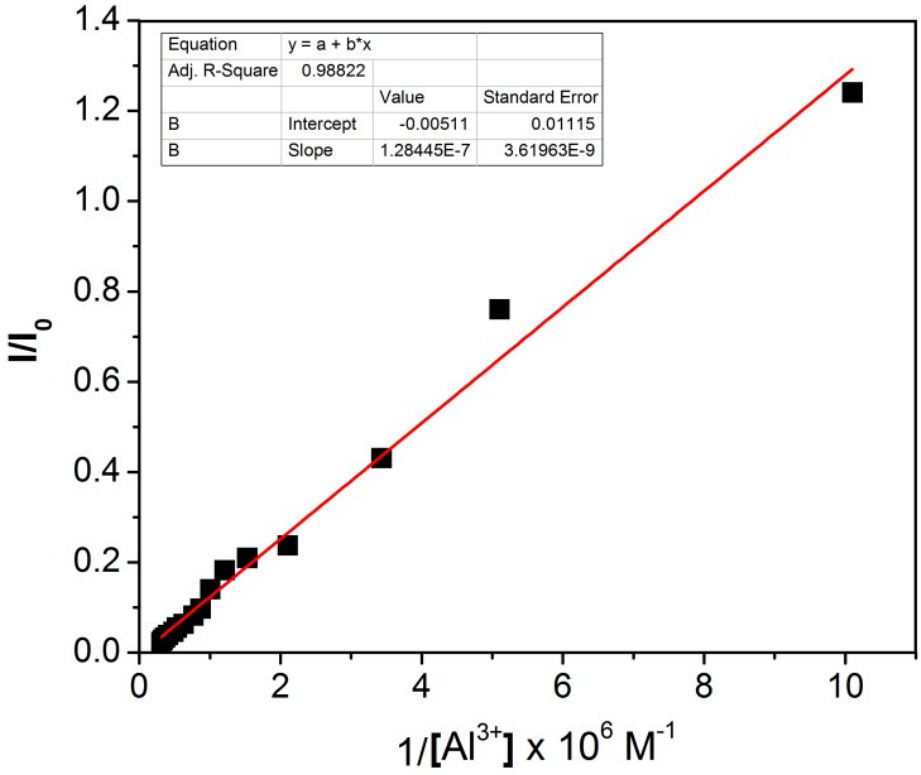

Figure S6. Calculation of association constant of Al^{3+} with **NPRB** by fluorescence titration method.

The association const. (K_a) of was determined from the equation: K_a = intercept/slope. From the linear fit graph we get, $K_a = 4 \times 10^4\ M^{-1}$ for Al^{3+} ion.

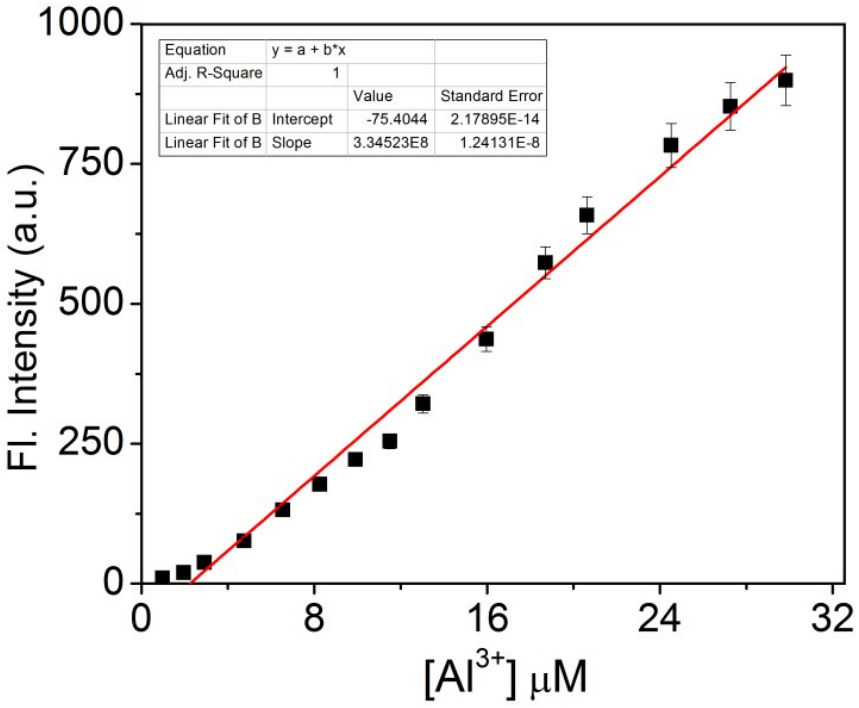

Figure S7. Fluorescence intensity plot of **NPRB** as a function of increasing Al^{3+} concentration. Each point of the plot represents the average of at least three independent binding constant values.

From the graph, we determined the Limit of Detection= 0.3 μM. Therefore **NPRB** can detect aluminium (III) up to this very lower concentration by fluorescence technique.

7. Job's plot for determining the stoichiometry of binding by fluorescence method:

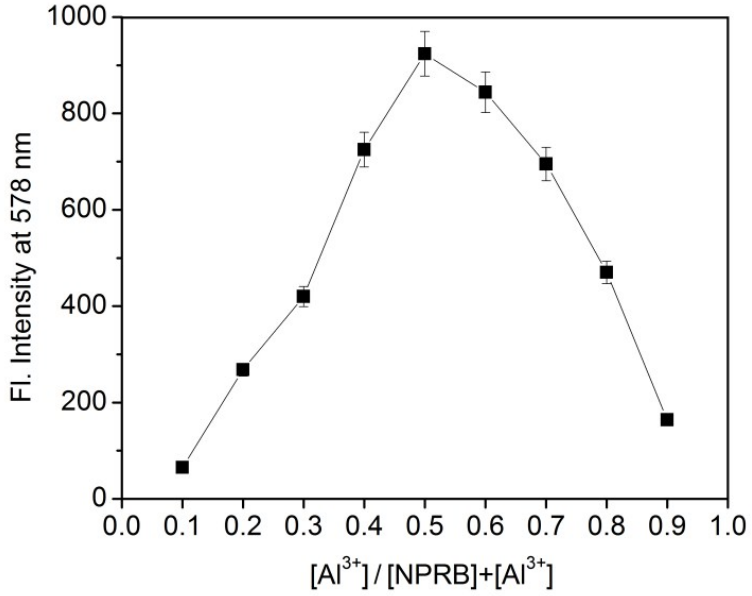

Figure S8. Job's plot for the complexation of **NPRB** with Al^{3+} in acetonitrile-water (1:8, v/v), neutral pH, ([**NPRB**] = [Al^{3+}] = 10 μM) by fluorescence method ($\lambda_{ex.}$= 490 nm). Error bars represent standard deviations (n = 3).

8. Comparative absorbance and fluorescence titration studies:

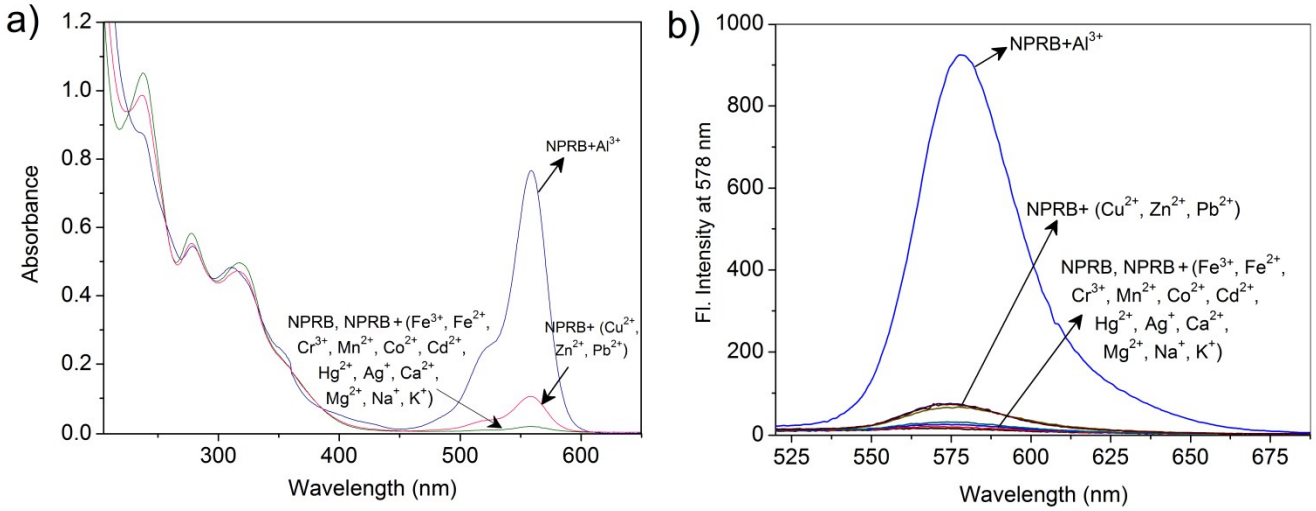

Figure S9. Comparative UV-vis absorption (a) and fluorescence (b) spectra of **NPRB** (10 μM) after addition of various biologically relevant metal cations upto 4 equiv. in CH_3CN/H_2O, 1:8 (v/v), (pH 7.2, 10 mM Tris-Cl buffer).

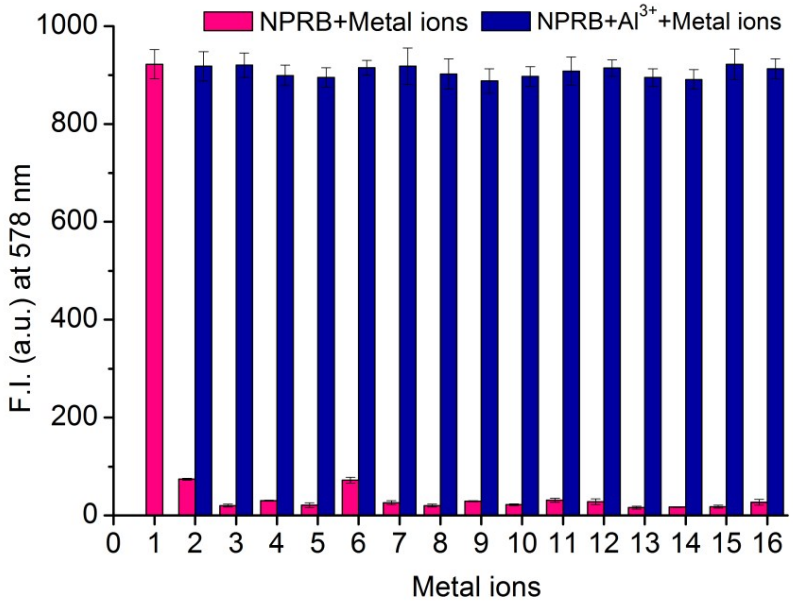

Figure S10. Fluorescence response of **NPRB** (10 μM) with various cations (4 equiv.) in CH_3CN/H_2O, 1:8 (v/v), (pH 7.2, 10 mM Tris-Cl buffer). Pink bars represent the responses of various metal ions towards **NPRB** and blue bars represents the responses of corresponding metal ions towards **NPRB** in presence of Al^{3+} [From left to right: 1. Al^{3+}, 2. Cu^{2+}, 3. Hg^{2+}, 4. Cd^{2+}, 5. Pb^{2+}, 6. Zn^{2+}, 7. Mg^{2+}, 8. Fe^{3+}, 9. Fe^{2+}, 10. Mn^{2+}, 11. Ni^{2+}, 12. Ag^{+}, 13. Ca^{2+}, 14. Co^{2+}, 15. Cr^{3+} and 16. Na^{+}].

9. Selectivity study of the probe NPRB with various biologically relevant analytes:

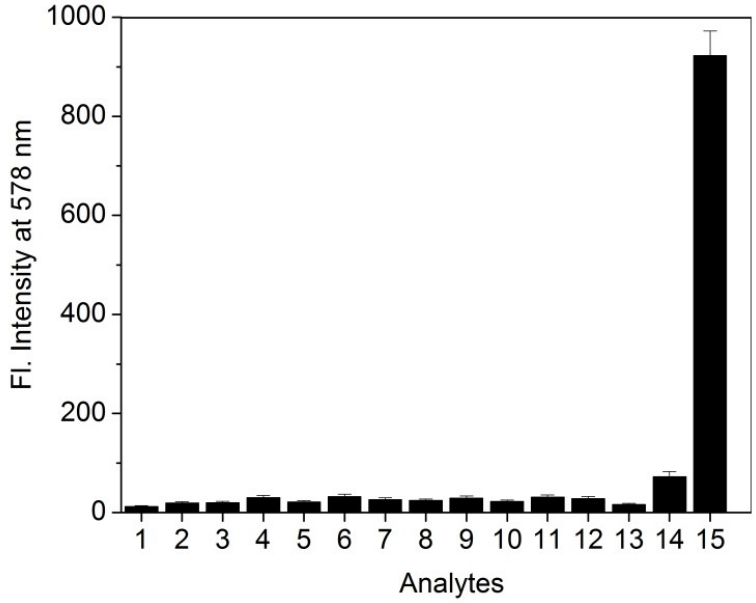

Figure S11: Comparative fluorescence response (λ_{ex}= 490 nm) of **NPRB** with different analytes i.e. 1. Blank, 2. Mg^{2+}, 3. Fe^{2+}, 4. $ONOO^-$, 5. H_2S, 6. CO, 7. NO, 8. H_2O_2, 9. Cl^-, 10. AcO^-, 11. NO_2^-, 12. SO_3^-,

13. ClO^-, 14. Cu^{2+} and 15. Al^{3+} in CH_3CN/H_2O, 1:8 (v/v) (pH 7.2, 10 mM Tris-Cl buffer). Standard deviations are represented by error bars (n=3).

10. Fluorescence response of NPRB towards Al^{3+} in solid phase:

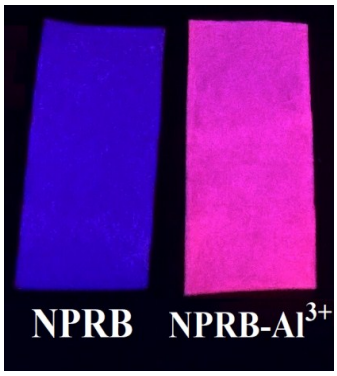

Figure S12. Fluorescence color change of paper strip soaked in **NPRB** solution after addition of Al^{3+} in solid phase.

11. Dependence of NPRB on the anionic parts of the Al^{3+} salts:

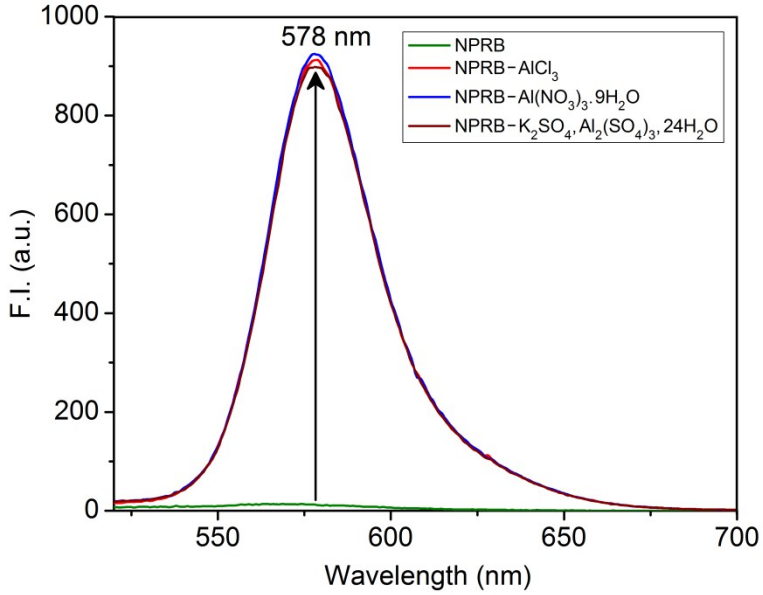

Figure S12. Fluorescence intensities of **NPRB** after addition of various Al^{3+} salts with different anionic parts in CH_3CN/H_2O, 1:8 (v/v) (pH 7.2, 10 mM Tris-Cl buffer).

12. Reversibility of the probe NPRB-Al^{3+} complex with EDTA:

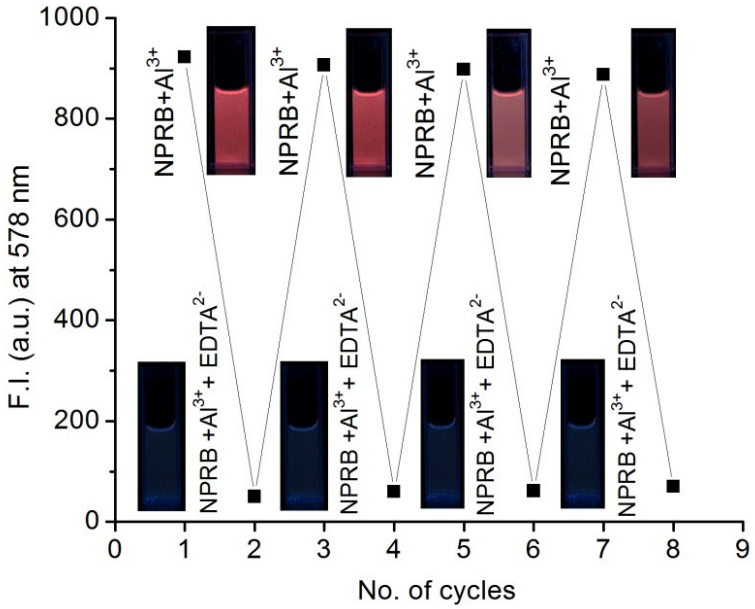

Figure S13. Fluorescence intensity plot of **NPRB-Al^{3+}** complex showing the reversibility of the complex with EDTA upto eight cycles.

13. pH titration curve of NPRB upon gradual addition of Al^{3+}:

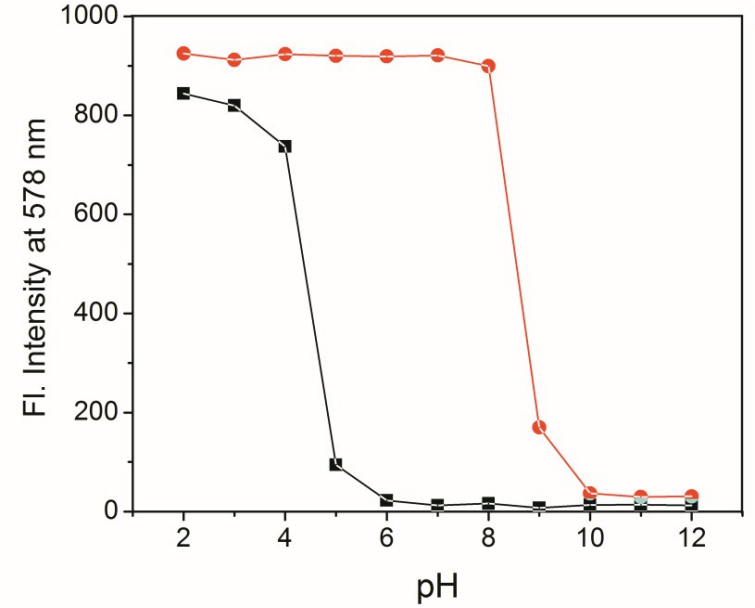

Figure S14. Fluorescence responses of probe **NPRB** (black) and **NPRB**-Al^{3+} complex (red) in different pH conditions in CH_3CN/H_2O (1:8, v/v) (λ_{ex}= 490 nm).

14. ^{1}H NMR titration spectrum of NPRB with Al^{3+}:

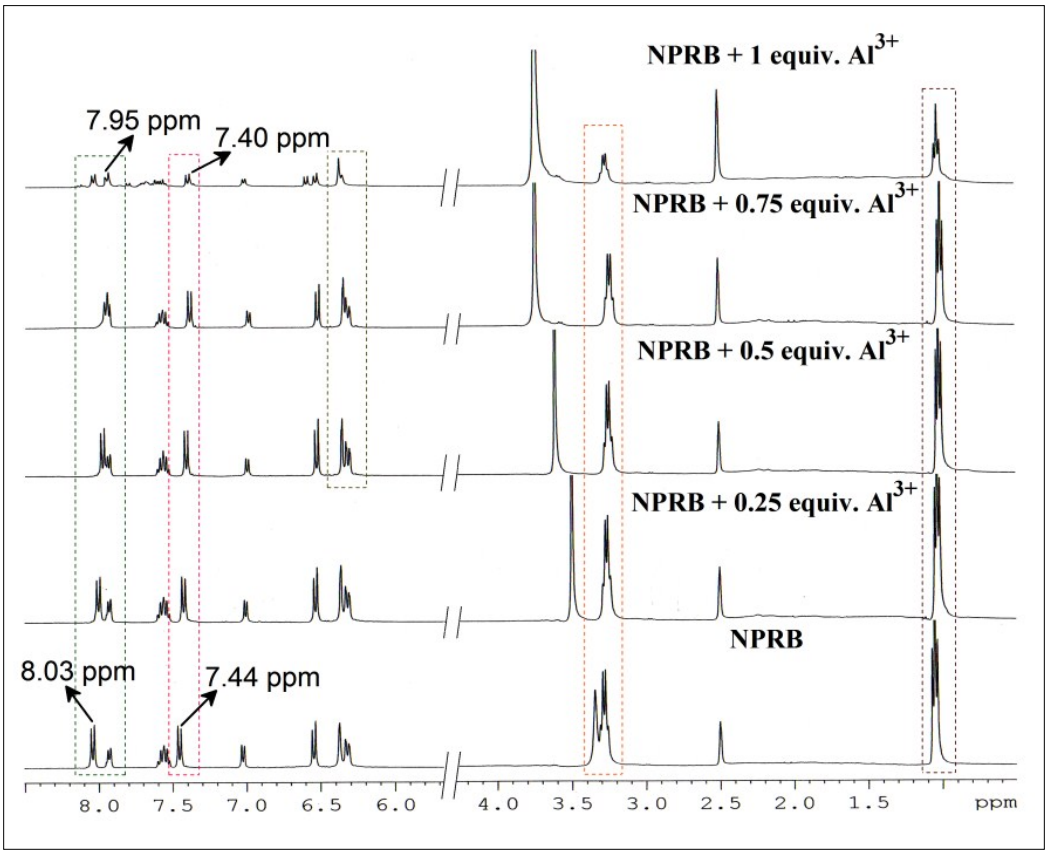

Figure S15. Partial ^{1}H NMR titration [400 MHz] of **NPRB** in DMSO-d_6 at 25^0C and the corresponding changes after the gradual addition of one equiv. of Al^{3+} in D_2O.

15. ^{13}C NMR titration spectrum of NPRB with Al^{3+}:

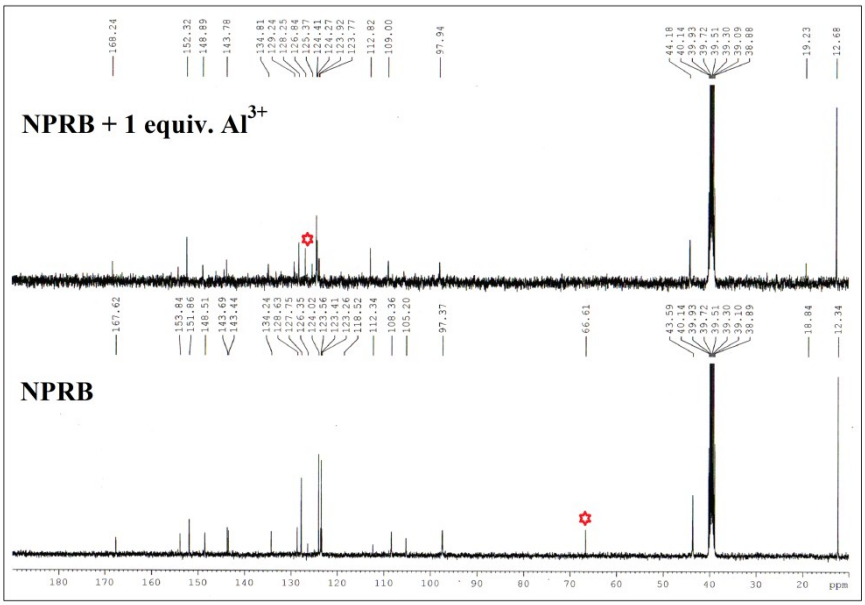

Figure S16. ^{13}C NMR titration [400 MHz] of **NPRB** in DMSO-d_6 at 25^{0}C (below) and the corresponding changes after the gradual addition of one equiv. of Al^{3+} in D_2O (above).

16. Partial HRMS titration spectrum of NPRB with Al^{3+}:

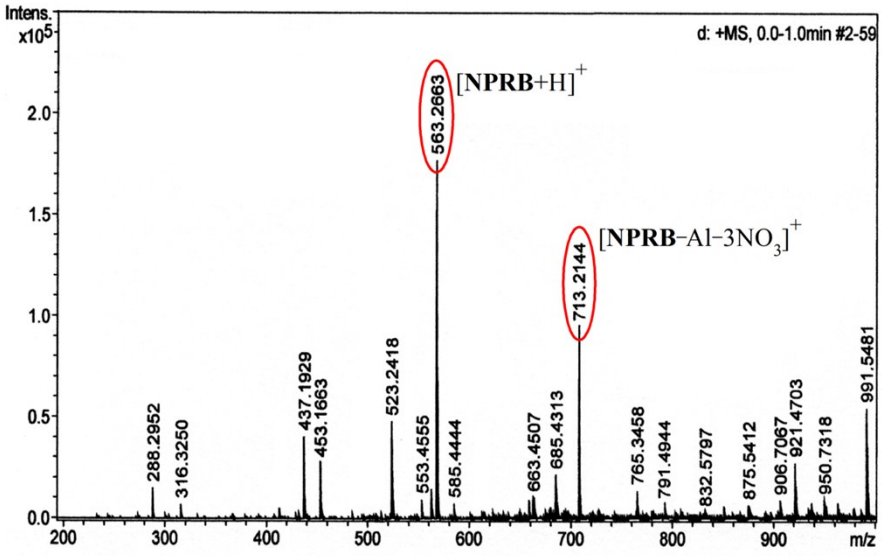

Figure S17. Partial ESI-MS spectra of **NPRB**-Al^{3+} complex in acetonitrile, taken after two hours of mixing.

17. Details of energy calculations using Density Functional Theory (DFT):

Table S2. Details of the geometry optimization in Gaussian 09 program.

Details	NPRB	NPRB-Al^{3+} complex
Calculation method	RB3LYP	RB3LYP
Basis set	6-31G**	6-31G**/LANL2DZ
E(RB3LYP) (a.u.)	-1836.000	-2399.136
Charge, Multiplicity	0, 1	1, 1
Solvent (CPCM)	Water	Water

Table S3. Selected electronic excitation energies (eV), oscillator strengths (f), main configurations of the low-lying excited states of the probe and complex.

Molecules	Electronic Transition	Excitation Energy[a]	f[b]	Composition[c](%)
NPRB	$S_0 \rightarrow S_6$	3.6054 eV 350.11 nm	0.6078	H-3 → L (70 %)
	$S_0 \rightarrow S_{16}$	4.2746 eV 290.05 nm	0.2357	H → L+4 (63 %)
NPRB-Al^{3+}	$S_0 \rightarrow S_5$	2.6319 eV 471.09 nm	0.9472	H → L+2 (69.3 %)
	$S_0 \rightarrow S_8$	3.1322 eV 395.83 nm	0.3640	H-1 → L+2 (55.7 %)

[a]Only selected excited states were considered. The numbers in parentheses are the excitation energy in wavelength.[b]Oscillator strength. [c]H stands for HOMO and L stands for LUMO.

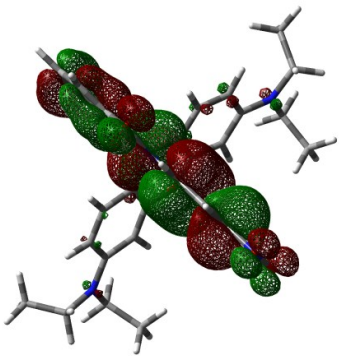

NPRB (HOMO-3)

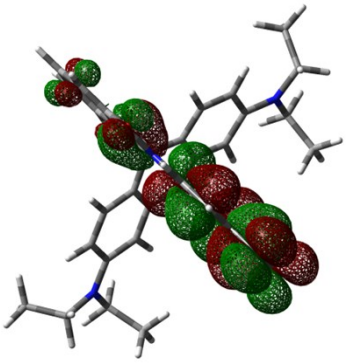

NPRB (LUMO)

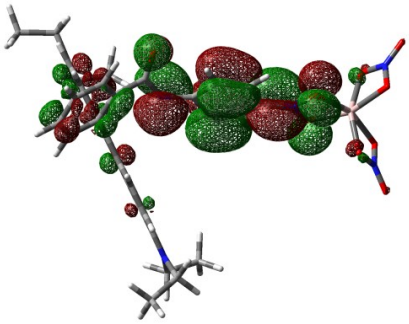

NPRB-Al^{3+} (HOMO)

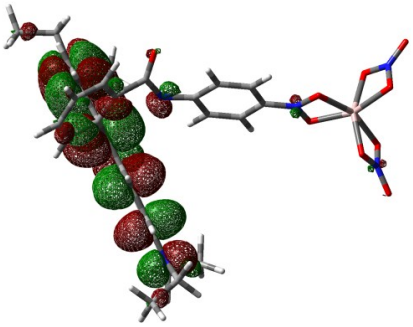

NPRB-Al^{3+} (LUMO+2)

Figure S18. Molecular orbitals and electronic contribution of the relevant excitations of **NPRB** (above) and **NPRB-**Al^{3+} complex (below).

Table S4. Energies of the highest occupied molecular orbital (HOMO) and lowest unoccupied molecular orbital (LUMO).

Species	E_{HOMO} (a.u)	E_{LUMO} (a.u)	ΔE(a.u)	ΔE(eV)	ΔE(kcal/mol)
NPRB	-0.23822	-0.09157	0.14665	3.98	92.00
NPRB -Al^{3+}	-0.21500	-0.10976	0.10524	2.86	65.95

18. Methodology for the imaging of zebrafish brain tissue:

Live specimens of adult (>6 months old), wild-type, male zebrafish, *Danio rerio* (Actinopterygii, Cypriniformes, Cyprinidae) were maintained in the laboratory conditions at 28°C under 14/10 h light/dark cycle as described earlier (Westerfield, 1995; Das et al., 2013, Maitra et al., 2014). All animal experiments were carried out following the guidelines of Institutional Animal Ethics Committee (Reg. no.: 1819/GO/Ere/S/15/CPCSEA) of Visva-Bharati University. We also confirm that all the experiments were performed in accordance with the relevant guidelines and regulations. During autopsy live specimens (6-10 fish per treatment group) were anesthetized by immersion into 0.1% 3-aminobenzoic acid ethyl ester methane sulfonate salt (MS-222; Sigma) in fresh water, killed by decapitation; brain was dissected out and placed immediately in ice chilled phosphate buffer saline, PBS (0.1M phosphate buffer; pH 7.4 containing 0.6% NaCl and 0.01% Triton X-100). Zebrafish brain, specifically the telencephalon, optic tectum, optic chiasma, hypothalamus and medulla oblongata were sliced using sharp blades under a stereozoom microscope (Zoomster 6, Dewinter Optical Inc., Italy) and incubated in 6 well culture plate (Nunc, India) either in PBS alone or supplemented with the guest, $Al(NO_3)_3$ (50 μM) for 60 min in a humidified chamber at 23 ± 2°C. Brain slices were washed (3x) with chilled PBS, probed with the NPRB (10 μM) for 15 min with gentle shaking (40 rpm), washed again to remove unbound probe and observed under an inverted fluorescent microscope (DMi8, Leica Microsystems, Germany) using HI PLAN I 10x/0.22 PH1 objective and ROHD filter (excitation and emission ranges at 520 nm and 580 nm respectively). Images were acquired through Leica EC4 Digital Camera and DFC 3000G and processed using LAS X software.